CHEMISTRY
A EUROPEAN JOURNAL

DOI: 10.1002/chem.201101509

Persistent Hydrogen-Bonded and Non-Hydrogen-Bonded Phenoxyl Radicals

Riccardo Wanke,[a] Laurent Benisvy,*[b] Maxim L. Kuznetsov,[a] M. Fátima C. Guedes da Silva,[a, c] and Armando J. L. Pombeiro*[a]

Abstract: The production of stable phenoxyl radicals is undoubtedly a synthetic chemical challenge. Yet it is a useful way to gain information on the properties of the biological tyrosyl radicals. Recently, several persistent phenoxyl radicals have been reported, but only limited synthetic variations could be achieved. Herein, we show that the amide–*o*-substituted phenoxyl radical (i.e. with a salicylamide backbone) can be synthesised in a stable manner, thereby permitting easy synthetic modifications to be made through the amide bond. To study the effect of H-bonding on the properties of the phenolate/phenoxyl radical redox couple, simple H-bonded and non-H-bonded *o*,*p*-*t*Bu-protected salicylamidate compounds have been prepared. Their redox properties were examined by cyclic voltammetry and showed a fully reversible one-electron oxidation process to the corresponding phenoxyl radical species. Remarkably, the redox potential appears to be correlated, at least partially, with H-bond strength, as relatively large differences (ca. 300 mV) in the redox potential between H-bonded and non-H-bonded phenolate salts are observed. The corresponding phenoxyl radicals produced electrochemically are persistent at room temperature for at least an hour; their UV/Vis and EPR characterisation is consistent with that of phenoxyl radicals, which makes them excellent models of biological tyrosyl radicals. The analyses of the experimental data coupled with theoretical calculations indicate that both the deviation from planarity of the amide function and intramolecular H-bonding influence the oxidation potential of the phenolate. The latter H-bonding effect appears to be predominantly exerted on the phenolate and not (or only a little) on the phenoxyl radical. Thus, in these systems the H-bonding energy involved in the phenoxyl radical appears to be relatively small.

Keywords: electron transfer · hydrogen bonds · phenol · phenolate · phenoxyl radicals · redox chemistry · tyrosyl radical model

Introduction

Tyrosyl radicals (Tyr$^{\bullet}$) play a crucial role in many biological systems.[1] For instance, they are essential to the catalytic activity of: 1) the class I RNR (iron-dependent ribonucleotide reductase) enzymes that are relevant in DNA replication and DNA repair, and 2) the photosystem II (PSII) that uses sunlight to split water into O_2 through photosynthesis. In class I RNR, a free Tyr$^{\bullet}$ is produced in the proximity of a diiron core, whereas in PSII a Tyr$^{\bullet}$ H-bonded to an adjacent histidine residue is formed. H-bonding is suspected to have a strong influence on the redox properties of the tyrosine; indeed, whilst the redox potential of Tyr/Tyr$^{\bullet}$ (versus the normal hydrogen electrode) has a value of 1.00 V for the non-hydrogen-bonded Tyr_{122} of RNR,[2] it decreases significantly to 0.72–0.76 V for the H-bonded Tyr_D in PSII.[3] These observations pose fundamental questions on the influence of H-bonding on the redox properties (and mechanism of formation) of the biological Tyr$^{\bullet}$.

In less than a decade, remarkable synthetic progress has been made in generating and characterising persistent H-bonded phenoxyl radicals as chemical models for biological Tyr radicals. For instance, *o*,*p*-*t*Bu-protected phenol compounds that are intramolecularly H-bonded to a nitrogen base (from amino, imidazole or pyridine groups) have proved to undergo a (quasi)reversible proton-coupled electron transfer (PCET) oxidation process to H-bonded phenoxyl radicals of the type R–O$^{\bullet}$···H–$^{+}$N.[4–14] In these systems, the phenol oxidation process occurs at a much lower potential than that of a non-H-bonded phenol, which could, at first sight, be a consequence of H-bonding effects in the reduced and oxidised forms. However, Mayer and co-workers have elegantly demonstrated that this decrease in redox potential results predominantly from the driving force for proton movement in a concerted PCET (i.e. CPET) mecha-

[a] Dr. R. Wanke, Dr. M. L. Kuznetsov, Dr. M. F. C. Guedes da Silva, Prof. A. J. L. Pombeiro
Centro de Química Estrutural, Complexo I
Instituto Superior Técnico, TU, Lisbon
Avenida Rovisco Pais, 1049-001 Lisbon (Portugal)
Fax: (+351) 21-846-4455
E-mail: pombeiro@ist.utl.pt

[b] Dr. L. Benisvy
Department of Chemistry, Laboratory of Biomimetic Chemistry
Bar-Ilan University, Ramat Gan 52900 (Israel)
Fax: (+972) 3-7384053
E-mail: benisvl@mail.biu.ac.il

[c] Dr. M. F. C. Guedes da Silva
Universidade Lusófona de Humanidades e Tecnologias, Lisbon
Av. Campo Grande 376, 1749-024 Lisbon (Portugal)

Supporting information for this article is available on the WWW under http://dx.doi.org/10.1002/chem.201101509.

nism.[11,15] Thus, although these systems are excellent models for mechanistic studies on PCET, the associated proton movement during oxidation prevents direct insights into the effects of H-bonding on the phenoxyl redox potential. With the aim of studying the "real" effect of H-bonding on the phenolate/phenoxyl radical redox couple, we have designed new, simple, *o*,*p*-*t*Bu-protected salicylamidate compounds ($^{RR'}L^-$; Scheme 1), which comprise (or not) a (phenolate)O$^-$···H–N(amide) intramolecular H bond. Herein, we show that both H-bonded and non-H-bonded phenolate compounds undergo a straightforward one-electron reversible oxidation process (ET process) to the corresponding persistent phenoxyl radical species, which indicates that the salicylamide backbone can be used to produce stable phenoxyl radicals. Thus, in these systems, the oxidation process does not involve any proton transfer and yet allows H-bonding (or not) at both the phenolate and phenoxyl radical. The redox potential of this process is shown to be affected by both the deviation of the amide backbone from planarity and the presence of H-bonding, the effect of which is predominantly exerted on the phenolate.

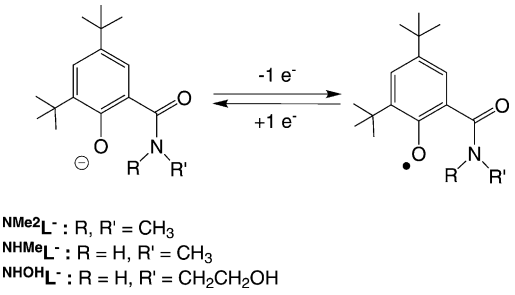

Scheme 1.

Results and Discussion

Synthesis of $^{NRR'}$LH and [$^{NRR'}$L][NBu$_4$]: The phenols $^{NRR'}$LH (Scheme 1) are readily synthesised in high yield[16] by the condensation of the corresponding amine, HNRR′, onto succinimide-activated 3,5-di-*tert*-butyl salicylic acid. The deprotonation of the phenol moiety by using an equimolar amount of OH[NBu$_4$] yields the corresponding phenolate salt, [$^{NRR'}$L][NBu$_4$].

Solid, solution and calculated structures $^{NRR'}$LH and their corresponding phenolate salts [$^{NRR'}$L][NBu$_4$]: It is well known that 2-phenol amide compounds commonly exhibit a planar conformation owing to strong intramolecular O–H···O H-bonding between the phenol O–H and the adjacent carbonyl O atom. Kanamori et al.[17] have elegantly shown that deprotonation of the phenol group induces a conformation twist of the amide function, thereby yielding a planar structure characterised by strong intramolecular O$^-$···H–N H-bonding between the phenolate O$^-$ atom and the amide N–H, as illustrated in Scheme 2. Clearly for secondary amines (that do not possess the N–H amide function), whilst intramolecular H-bonding can occur in the phenol form, it cannot in the phenolate form. This constitutes the basis of our strategy in building H-bonding versus non-H-bonding phenolate compounds (Scheme 1).

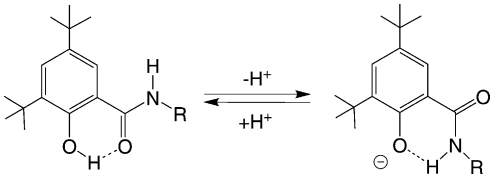

Scheme 2. Conformational twist upon deprotonation of 2-phenol amide compounds.

Planar H-bonded phenols ^{NHOH}LH and ^{NHMe}LH and their corresponding H-bonded phenolate salts [^{NHOH}L][NBu$_4$] and [^{NHMe}L][NBu$_4$]: The structures of the phenol and phenolate compounds described herein have been studied in solution by NMR and IR spectroscopy, in the gas phase by DFT calculations, and in the solid state by X-ray crystallography for ^{NHOH}LH*, [^{NHOH}L][NBu$_4$] and [^{NHMe}L][NBu$_4$] (see Tables 1 and 2, Figures 1 and 2). The X-ray structure of phenol ^{NHOH}LH* (analogue to ^{NHOH}LH but lacking *t*Bu groups,

Table 1. Crystallographic data for ^{NMe2}LH, ^{NHOH}LH*, [^{NHOH}L][NBu$_4$]·2H$_2$O and [^{NHMe}L]$^-$.

	^{NMe2}LH	^{NHOH}LH*	[^{NHOH}L][NBu$_4$]·2H$_2$O	[^{NHMe}L]$^-$
formula	$C_{17}H_{27}N_1O_2$	$C_9H_{11}N_1O_3$	$C_{33}H_{66}N_2O_5$	$C_{16}H_{24}NO_2$
M	277.40	181.19	570.88	262.36
crystal system	triclinic	monoclinic	triclinic	monoclinic
space group	P$\bar{1}$ (No. 2)	*P*21/*c* (No. 14)	P$\bar{1}$ (No. 2)	*P*21/*c* (No. 14)
a [Å]	6.2379(6)	8.5549(8)	8.9498(12)	11.268(4)
b [Å]	16.1287(16)	12.1590(12)	13.4507(18)	16.369(6)
c [Å]	18.7725(19)	9.1001(10)	15.964(2)	19.073(7)
α [°]	110.978(4)	90.00	86.522(10)	90.00
β [°]	99.397(6)	115.466(2)	88.448(10)	115.31(2)
γ [°]	97.111(5)	90.00	72.232(9)	90.00
V [Å^3]	1705.4(3)	854.61(15)	1826.7(4)	3180 (2)
Z	4	4	2	4
ρ_{calcd} [g cm^{-3}]	1.080	1.408	1.038	0.548
μ [cm^{-1}]	0.070	0.106	0.068	0.036
reflections collected	22308	4306	23205	19075
unique reflections	6211	1872	6675	5799
R_{int}	0.0656	0.0469	0.0807	0.0640
observed reflections	3573	1429	3535	3004
R	0.0578	0.0404	0.0636	0.1043
R_w	0.117	0.0561	0.1352	0.1452

Table 2. Experimental and calculated geometrical parameters for phenol $^{NRR'}$LH, phenolate $^{NRR'}$L$^-$ and phenoxyl radical $^{NRR'}$L$^{\bullet}$ compounds (RR′ = Me_2, HMe, HOH).

Compound		^{NMe2}LH		^{NMe2}L$^-$	^{NMe2}L$^{\bullet}$	^{NHMe}LH	^{NHMe}L$^-$		^{NHMe}L$^{\bullet}$	^{NHOH}LH*, ^{NHOH}LH		^{NHOH}L$^-$		^{NHOH}L$^{\bullet}$
Method		expt	calcd	calcd	calcd	calcd	expt	calcd	calcd	expt	calcd	expt	calcd	calcd
Phenol–amide twist angle [°]		ca. 71	30	60	80									
			non-planar				< 10 planar					< 10 planar		
Intramolecular H-bonding		none	OH···O	none	none	OH···O	O$^-$···HN		O$^{\bullet}$···HN	OH···O		O$^-$···HN		O$^{\bullet}$···HN
bond length [Å]	C1–O1	1.374(3)	1.355	1.276	1.258	1.350	1.290(3)	1.291	1.260	1.3606(17)	1.349	1.303(3)	1.291	1.260
	C1–C2	1.395(3)	1.416	1.450	1.461	1.418	1.437(4)	1.447	1.467	1.4092(19)	1.419	1.426(4)	1.448	1.467
	C2–C3	1.392(3)	1.408	1.404	1.382	1.410	1.373(4)	1.404	1.381	1.4043(19)	1.411	1.399(4)	1.405	1.381
	C3–C4	1.379(3)	1.390	1.393	1.409	1.387	1.381(4)	1.391	1.410	1.376(2)	1.387	1.375(4)	1.390	1.411
	C4–C5	1.400(4)	1.411	1.417	1.424	1.412	1.402(4)	1.407	1.421	1.390(2)	1.412	1.406(4)	1.416	1.421
	C5–C6	1.387(4)	1.396	1.389	1.381	1.393	1.374(4)	1.390	1.380	1.382(2)	1.393	1.371(4)	1.389	1.380
	C6–C1	1.401(3)	1.421	1.466	1.474	1.424	1.433(4)	1.459	1.478	1.391(2)	1.424	1.444(4)	1.459	1.478
	C2–C7	1.501(3)	1.491	1.492	1.510	1.488	1.511(4)	1.494	1.517	1.4850(18)	1.389	1.482(4)	1.492	1.518
	C7–O2	1.243(3)	1.251	1.246	1.235	1.252	1.243(4)	1.250	1.237	1.2628(16)	1.252	1.251(3)	1.250	1.236
	C7–N1	1.334(3)	1.370	1.382	1.363	1.359	1.317(4)	1.361	1.352	1.3276(18)	1.361	1.331(3)	1.366	1.356
	C8–N1	1.468(3)	1.462	1.450	1.455	1.457	1.456(4)	1.443	1.452	1.4590(18)	1.459	1.443(4)	1.445	1.455
	(C9–N1)	(1.452(3))	(1.462)	1.448	1.458									

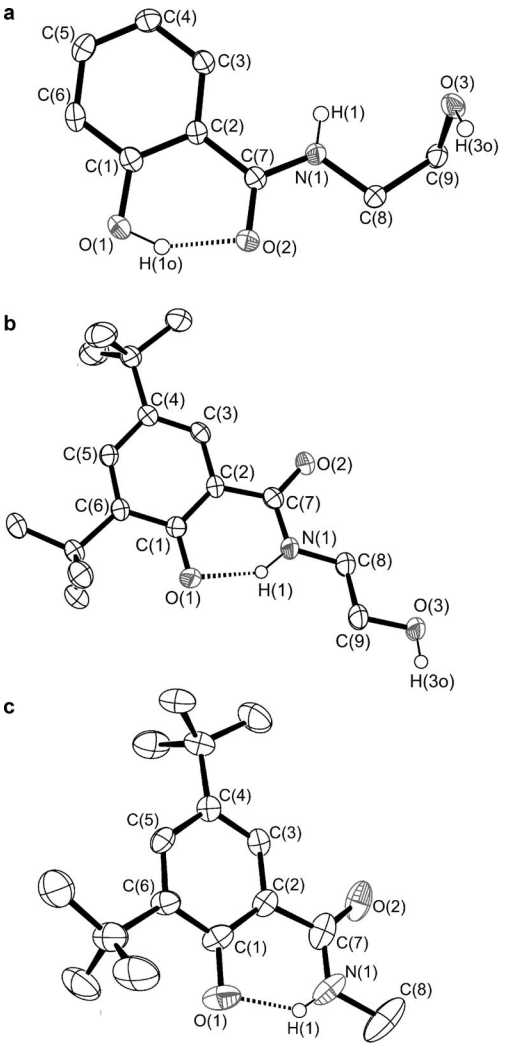

Figure 1. ORTEP representations (shown with 50% thermal ellipsoids) of ^{NHOH}LH* (a), ^{NHOH}L$^-$ in [^{NHOH}L][NBu_4]·$2H_2O$ (b) and ^{NHMe}L$^-$ in [^{NHMe}L][NBu_4] (c). Only the H atoms of NH and OH groups are shown.

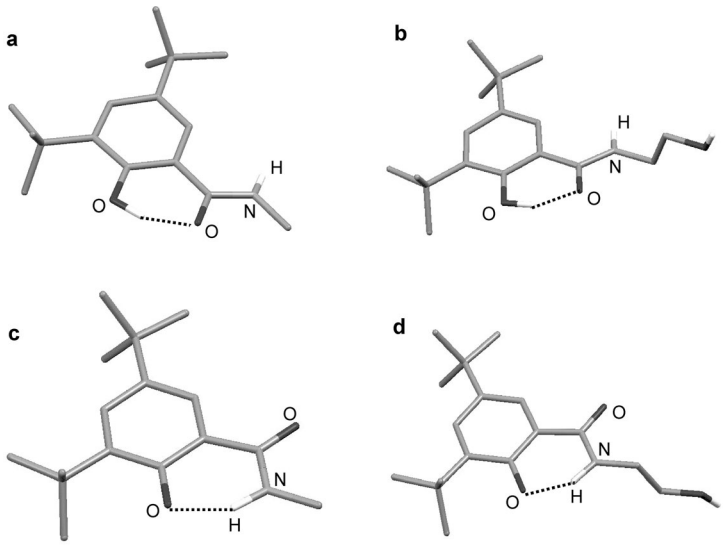

Figure 2. DFT-calculated structures of ^{NHMe}LH (a), ^{NHOH}LH (b), ^{NHMe}L$^-$ (c) and ^{NHOH}L$^-$ (d).

Figure 1), as expected, reveals a planar conformation (dihedral angle 14.02°) owing to the O–H···O H-bonding between the phenol O–H and the adjacent carbonyl O atom. The parameters (O···O distance, O–H···O angle) are as expected and are comparable to those of other 2-amide phenol compounds.[18] The ^{1}H NMR spectra of ^{NHOH}LH and ^{NHMe}LH, in CD_3CN, exhibit a phenolic O–H proton resonance at δ = 13.31 and 13.39 ppm, respectively, characteristic of an O–H···O=C intramolecular H bond of the phenol,[17,18] whereas the amide N–H proton resonances at δ = 7.49 and 7.37 ppm, respectively, are typical for a non-hydrogen-bonded amide N–H. Moreover, the IR spectra of ^{NHOH}LH and ^{NHMe}LH, in CH_3CN solution, exhibit an N–H stretching frequency at 3411 and 3413 cm^{-1}, respectively, typical of a non-H-bonded amide N–H. Thus, these data clearly demonstrate that the

phenol ^{NHOH}LH and ^{NHMe}LH possess a planar conformation with OH···O H-bonding in the solid state as well as in solution. The molecular structures of the phenolate salts [^{NHOH}L][NBu_4]·$2H_2O$[19] and [^{NHMe}L][NBu_4], as revealed by X-ray crystallography (Figure 1), are quasi-planar with twist angles between the phenolate and the CONH moiety of 6.86° in [^{NHOH}L][NBu_4]·$2H_2O$ and 5.52° in [^{NHMe}L][NBu_4]. The planarity of both phenolate compounds results from relatively strong intramolecular O^-···H–N H-bonding[20] involving the phenolate O atom and the adjacent N–H amide group, as evidenced by the O···N distance and the O···H–N angle in [^{NHOH}L][NBu_4]·$2H_2O$ (2.585 Å and 145.59°) and in [^{NHMe}L]-[NBu_4] (2.573 Å and 139.36°), which are comparable to those of other O^-(oxyanion)···H–N-(amide)/H–O(carboxylic) intramolecularly H-bonded salicylamidate[17,18,21]/salicylate[22] compounds. The bond lengths and angles within both structures are as expected for phenolate compounds,[18] with a C–O bond length of 1.303(3) Å (in $^{NHOH}L^-$) and 1.290(3) Å (in $^{NHMe}L^-$; see Table 2). The ^{1}H NMR spectra of the phenolate salts [^{NHOH}L][NBu_4] and [^{NHMe}L][NBu_4] in CD_3CN each display a N–H resonance at a much lower field (i.e. at $\delta =$ 13.90 and 13.20 ppm, respectively) than that of the corresponding parent phenol ($\delta = 7.49$ and 7.37 ppm, respectively), clearly indicating that the N–H proton is involved in an intramolecular O^-···H–N hydrogen bond, as shown in Scheme 2.[18] Moreover, the IR spectra of $^{NHOH}L^-$ and $^{NHMe}L^-$, in CH_3CN solution, exhibit an N–H stretching at a much lower frequency (3005 and 3009 cm^{-1}, respectively) than that of the corresponding phenol (3411 and 3413 cm^{-1}), which is typically indicative of a relatively strongly H-bonded N–H bond.[19] Thus, these data clearly demonstrate that the O^-···H–N H-bonding identified in the X-ray structure of $^{NHOH}L^-$ and $^{NHMe}L^-$ is preserved in solution.

DFT calculations have been performed on the phenol and corresponding phenolate compounds. The calculated optimised structures are in good agreement with the corresponding structures determined experimentally. As shown in Table 2, the maximum difference between the calculated and experimental bond lengths is 0.03 Å and often falls within a 3σ interval of the experimental data. Additionally, the optimised structures of phenols ^{NHOH}LH and ^{NHMe}LH are planar and present intra-OH···O H-bonding; in addition, the optimised structures of phenolates $^{NHOH}L^-$ and $^{NHMe}L^-$ are planar with intra-O^-···HN H-bonding (see Figure 2, Table 2). Thus, these calculations reproduce well the solid-state and solution structures determined experimentally.

Non-planar phenol ^{NMe2}LH and its corresponding phenolate salt [^{NMe2}L][NBu_4]: The structures of the phenol ^{NMe2}LH and its corresponding phenolate [^{NMe2}L][NBu_4] salt have been studied in solution by NMR and IR spectroscopy, in the gas phase by DFT calculation, and in the solid state by X-ray crystallography for ^{NMe2}LH (Figures 3 and 4, Tables 1 and 2).

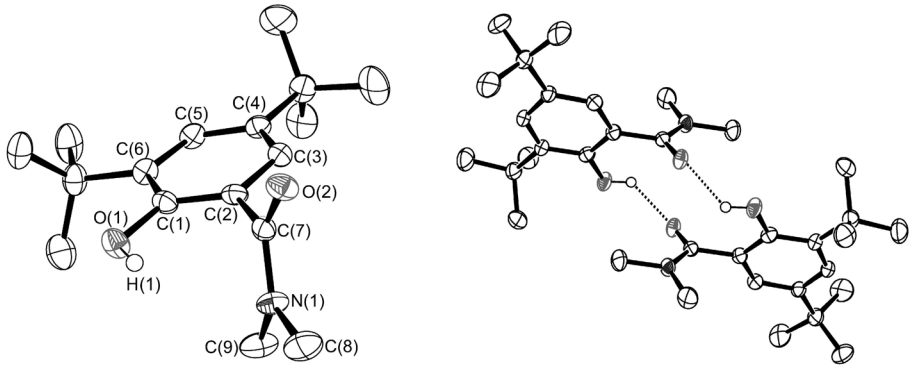

Figure 3. ORTEP representations (with 50% thermal ellipsoids) of ^{NMe2}LH showing the dimers formed through intermolecular OH···O bonding. Only the H atoms of OH groups are shown.

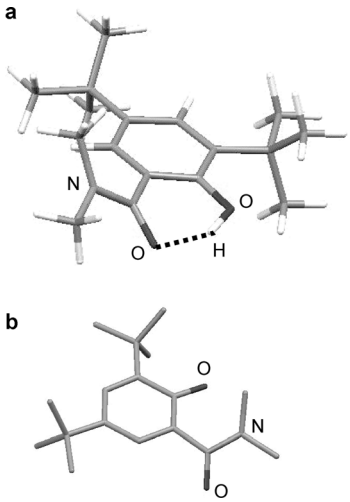

Figure 4. DFT-calculated structures of ^{NMe2}LH (a) and $^{NMe2}L^-$ (b).

The crystal structure of ^{NMe2}LH is in great contrast to that of ^{NHOH}LH*. Two molecules were found in the asymmetric unit, and the phenol ring and the amide backbone in each are no longer coplanar; instead, the O=C–$N(Me)_2$ planes are quasi-perpendicular to the phenol planes, with dihedral angles between the two planes of 71.18 and 71.77° (Figure 3). Thus, the intramolecular O–H···O=C H-bonding is prevented. Instead, both the phenol O–H and the C=O group act as H-bond donor and acceptor to another molecule, thus yielding dimer assemblies (Figure 3). The twist of the amide backbone is most likely to have occurred as a result of a steric clash between one of the two methyl groups and the nearby *meta* proton, which prevents the molecule from being planar. Thus, in ^{NMe2}LH, not only is the in-

tramolecular O–H···O=C bonding lost, but also the delocalisation of the π system is disrupted. However, this may be the result of crystal packing and the preferred arrangement of the molecules in crystals.

In solution, the ^{1}H NMR spectrum of ^{NMe2}LH, in CD_3CN, exhibits a phenolic O–H proton resonance at $\delta = 10.33$ ppm, which is shifted upfield relative to the H-bonded ^{NHOH}LH and ^{NHMe}LH (13.31 and 13.39 ppm, respectively). Nevertheless, the resonance at 10.33 ppm is far too high to be considered as the result of a proton resonance from a non-hydrogen-bonded phenol OH group. Moreover, the strong possibility of intermolecular H-bonding has been discarded, because this resonance has been found to be independent of sample dilution (with dilution of 1:100). Therefore, despite the steric hindrance imposed by the methyl groups, it appears that in solution intramolecular hydrogen bonding still occurs, to a weaker extent than for ^{NHOH}LH and ^{NHMe}LH. The DFT-calculated optimised structure appears to match the NMR data. Indeed, the optimised structure shows a phenol–amide twist angle of only about 30° and still permits relatively strong O–H···O=C intramolecular H-bonding (see Figure 4, Table 2), as well as minimising steric clashes between a methyl group and a *meta* proton. Thus, whilst the introduction of a supplementary methyl group at the amide function induces a twist and to some degree disrupts the extended π system, intramolecular H-bonding is evidenced in solution and confirmed by DFT calculation. The crystal structure presumably represents an extreme case in which optimisation of crystal packing and intermolecular H-bonding may have introduced further twisting.

The structure of the corresponding phenolate anion ^{NMe2}L$^-$ was estimated by DFT calculation. The optimised calculated structure reveals a large deviation from planarity, with a twist angle between the phenolate and the amide planes of approximately 60° (see Figure 4). This confirms that, as compared to [^{NHMe}L][NBu_4] and [^{NHOH}L][NBu_4], the loss of H-bonding by the introduction of a methyl group is also accompanied by a partial disruption of the delocalisation of the π system by the loss of planarity, and both effects should be taken into account (see below).

Electrochemical studies of [$^{NRR'}$L][NBu_4]: The cyclic voltammogram of each phenolate salt [$^{NRR'}$L][NBu_4], in CH_3CN at 298 K, exhibits a fully reversible one-electron oxidation process attributed to the formation of the corresponding phenoxyl radical species (Scheme 1, Figure 5). This oxidation process occurs at $E_{1/2} = -0.119$, -0.161 and -0.423 V versus ferrocene/ferrocenium (Fc/Fc^+) for ^{NHOH}L$^-$, ^{NHMe}L$^-$ and ^{NMe2}L$^-$, respectively. The full reversibility of the oxidation process of ^{NHOH}L$^-$ and ^{NHMe}L$^-$ most likely indicates the retention of the N–H···($^-$/$^{\bullet}$O) H bond upon oxidation, and presumably very little conformational change between reduced and oxidised species. The oxidation potentials of ^{NHOH}L$^-$ and ^{NHMe}L$^-$ are comparable to that of the previously reported 2-amido-4,6-di-*tert*-butylphenol recorded in water/CH_3CN under basic conditions (pH > 12).[24] In contrast, the oxidation of the non-hydrogen-bonded phenolate ^{NMe2}L$^-$

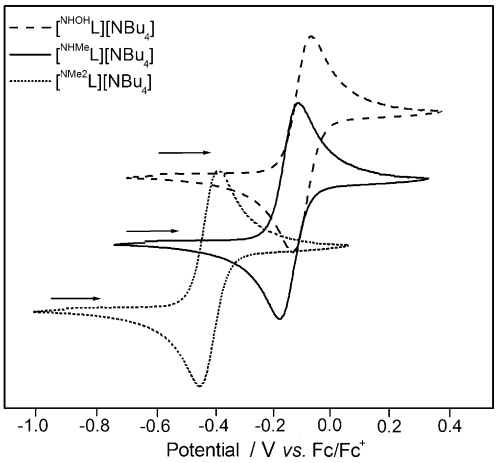

Figure 5. Cyclic voltammograms of [$^{NRR'}$L][NBu_4] (ca. 1 mM) in CH_3CN containing 0.2 M [NBu_4][BF_4] at 298 K recorded at a scan rate of 0.1 V s^{-1}.

($E_{1/2} = -0.423$ V vs. Fc/Fc^+) occurs at a much lower potential than those for ^{NHOH}L$^-$ and ^{NHMe}L$^-$, but at a higher potential than that of the non-hydrogen-bonded 2,4,6-tri-*tert*-butylphenoxide ArO$^-$ ($E_{1/2} = -0.572$ V vs. Fc/Fc^+ in CH_3CN).[25] This can be explained by combining 1) the electron-donating effect of the additional *o*-*t*Bu group in ArO$^-$, which makes it easier to oxidise, and 2) the electron-withdrawing effect of the amide functionality in ^{NMe2}L$^-$, which decreases the electron density at the O atom in ^{NMe2}L$^-$ thus making it harder to oxidise. Both these effects contribute to increasing the oxidation potential of the phenolate in ^{NMe2}L$^-$ as compared to ArO$^-$. Most importantly, relatively large differences (262 and 304 mV, respectively) in the redox potentials are observed between planar H-bonded (^{NHMe}L$^-$ and ^{NHOH}L$^-$) and twisted non-H-bonded (^{NMe2}L$^-$) salts. This redox shift may result from both combining effects acting in concert: 1) an H-bonding effect that reduces the electron density at the phenolate O atom, thus making the oxidation potential increase for ^{NHMe}L$^-$ and ^{NHOH}L$^-$ relative to ^{NMe2}L$^-$; and 2) the disruption of the extension of the π system to the amide backbone in ^{NMe2}L$^-$, which increases the electron density at the phenolate O atom, thereby making it easier to oxidise relative to ^{NHMe}L$^-$ and ^{NHOH}L$^-$. One should note that this contrasts, at least in part, with the early assumptions that H-bonding does not induce a significant redox shift.[11]

Generation and characterisation of the neutral phenoxyl radicals $^{NRR'}$L$^{\bullet}$: The electrochemical one-electron oxidation of each $^{NRR'}$L$^-$ anion, in CH_3CN at room temperature, yields the corresponding stable (for several hours under inert atmosphere) bright-green-coloured phenoxyl radical species $^{NRR'}$L$^{\bullet}$, as indicated by their UV/Vis and EPR spectra (see below). The cyclic voltammogram of each of the radicals produced is identical to that of its parent salt, thus confirming the chemical reversibility of the oxidation process.

The X-band EPR spectrum of each of the electrogenerated $^{NRR'}$L$^{\bullet}$ species, both in fluid and frozen CH_3CN solutions,

exhibits an isotropic radical signal centred at $g_{iso}=2.0046$ ($^{NMe2}L^{\bullet}$), 2.0043 ($^{NHOH}L^{\bullet}$) or 2.0042 ($^{NHMe}L^{\bullet}$) with a peak-to-peak line width of 3–4 G (Figure 6). The relatively small line width of each signal most likely indicates that there is no significant coupling of the radical with the N atom from the amide function, thus implying that the unpaired electron is not (or to a very little extent) delocalised on the amide group. The X-band spectrum of $^{NMe2}L^{\bullet}$ is well resolved (at 271 K) and exhibits a three-line pattern, which has been successfully simulated with the inclusion of a hyperfine coupling of the electron spin with both *meta* protons of the phenoxyl ring ($a_{Hmeta1}=1.60$ G; $a_{Hmeta2}=1.45$ G; Figure 6). As expected for *o*,*p*-protected phenoxyl radicals, the hyperfine coupling with the *meta* protons is relatively small (i.e. <2 G),[23] in agreement with the odd-alternant pattern of phenoxyl radicals in which the electron density is mainly spread on the O atom, and both *ortho* and *para* positions of the phenoxyl ring. In contrast to that of $^{NMe2}L^{\bullet}$, the spectrum of $^{NHMe}L^{\bullet}$ is unresolved and lacks hyperfine features. However, the spectrum of $^{NHOH}L^{\bullet}$ exhibits a barely observable doublet. The latter pattern is reminiscent of that obtained in a peptide-linked phenoxyl radical, invoking the coupling with only one H_{meta} atom ($a_H=1.7$ G).[24] These observations most likely indicate that H-bonding induces a redistribution of the electron spin density, as demonstrated earlier by Lucarini et al.[26]

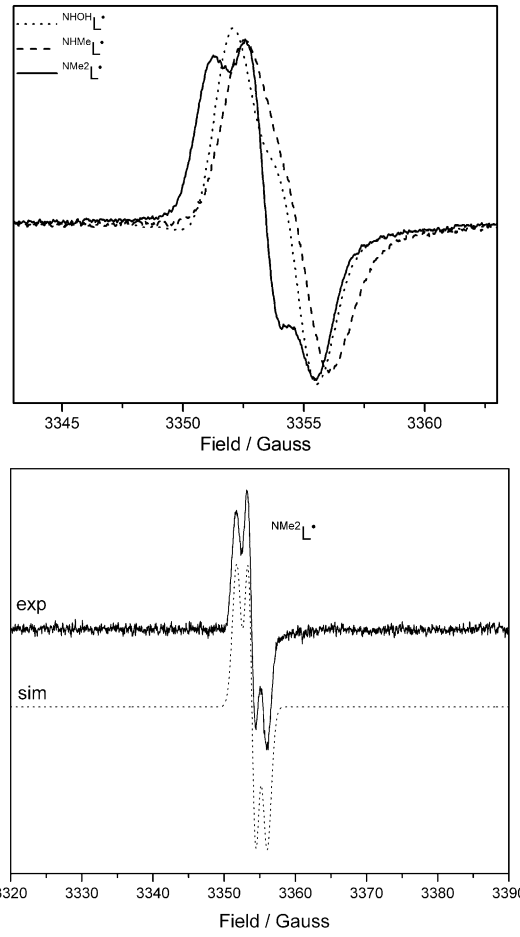

Figure 6. Top: X-band EPR spectra of electrogenerated radicals $^{NRR'}L^{\bullet}$ (ca. 1 mM) in CH_3CN containing $[NBu_4][BF_4]$ (0.2 M) recorded at 253–263 K. Bottom: X-band EPR spectrum (——) of the electrogenerated radical $^{NMe2}L^{\bullet}$ (ca. 1 mM) in CH_3CN containing $[NBu_4][BF_4]$ (0.2 M) recorded at 271 K; centre field: 3353.38; modulation frequency: 100 kHz; modulation amplitude: 0.3 Gpp; receiver gain: 4.48×10^{-4}; conversion time: 40.96 ms; microwave power: 0.4 mW; time constant: 81.92 ms; sweep time: 167.77 s. Simulated spectrum (•••••) obtained using Bruker SimFonia software, with the following fitting parameters: $g_x=g_y=g_z=2.0046$; $a_{H1meta}=1.60$ G; $a_{H2meta}=1.45$ G.

The UV/Vis spectrum of each electrogenerated oxidised species $^{NRR'}L^{\bullet}$ exhibits two intense bands at about 400 nm ($\varepsilon>1000\,M^{-1}cm^{-1}$) and a weak near-IR (NIR) broad band at 600–700 nm (ε ca. $250\,M^{-1}cm^{-1}$), which are characteristic of free or H-bonded phenoxyl radical transitions (Figure 7).[4,6,9,12,38] The ratio $\varepsilon_{400}/\varepsilon_{700}$ between the intensities of the approximately 400 nm (π–π^* transitions) and the circa 700 nm bands appeared to be indicative of the delocalisation of the phenoxyl unpaired electron; that is, for a "pure" phenoxyl radical, $\varepsilon_{400}/\varepsilon_{700}$ is about 5, whereas for a highly delocalised radical $\varepsilon_{400}/\varepsilon_{700}$ can even be <1.[9,38,39] Thus, the $\varepsilon_{400}/\varepsilon_{700}$ ratio of about 4 observed for each of the

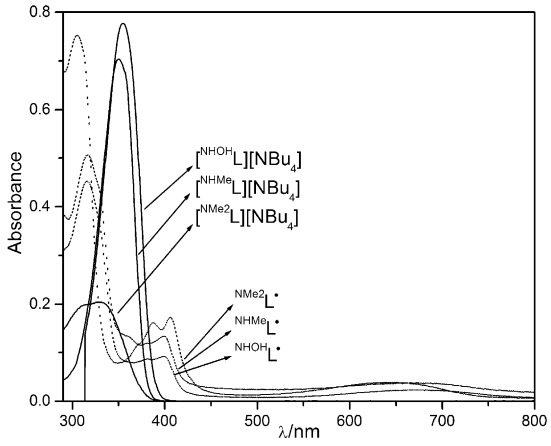

Figure 7. Room-temperature UV/Vis spectra of $[^{NRR'}L][NBu_4]$ (ca. 1 mM, ——) and their corresponding electrogenerated radicals $^{NRR'}L^{\bullet}$ (•••••), in CH_3CN containing $[NBu_4][BF_4]$ (0.2 M).

radicals studied strongly indicates that there is no or very little delocalisation of the unpaired electron in $^{NRR}L^{\bullet}$ onto the amide backbone, and that the electronic structure of each $^{NRR'}L^{\bullet}$ resembles that of a true phenoxyl radical.

DFT calculations were performed on the radical species to gain further information on their electronic structure. The geometry optimisation of $^{NHOH}L^{\bullet}$ and $^{NHMe}L^{\bullet}$ indicates a planar conformation allowing O$^{\bullet}\cdots$H–N H-bonding between the phenoxyl radical and the N–H amide, which confirms the reversible behaviour of the oxidation process from $^{NHR}L^{-}$ to $^{NHR}L^{\bullet}$. In contrast, the calculated structure of $^{NMe2}L^{\bullet}$ shows a twist of the amide function with respect to the phenoxyl plan. The twist angle is approximately 80°, essentially similar to its corresponding phenolate (twist angle 60°; see Table 2). Thus, it is likely that there is no (or only a little) conformation change between $^{NMe2}L^{-}$ and $^{NMe2}L^{\bullet}$. In all three radical species, the corresponding calculated bond lengths are considered to be essentially identical (see Table 2) and the calculated SOMO is characterised by a typical odd-alternant pattern of phenoxyl radicals. As a result, the electron spin density is quasi-equally distributed over both *ortho* and *para* C atoms and the phenoxyl O atom (see Figure 8),[27] and, as expected, very little electron spin density (<2%) is located on the amide N atom.

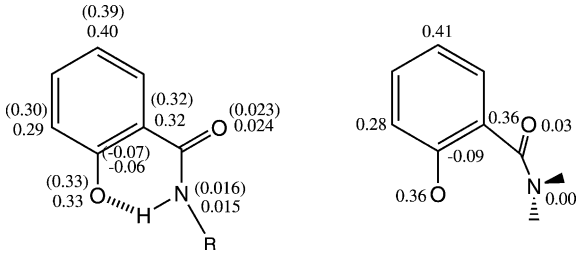

Figure 8. Calculated spin density distribution in (left) $^{NHOH}L^{\bullet}$ and $^{NHMe}L^{\bullet}$ (numbers in parentheses), and in (right) $^{NMe2}L^{\bullet}$.

H-bonding influence on the phenolate/phenoxyl radical redox couple: From the results described above, it is clear that both H-bonded phenolate compounds $^{NHMe}L^{-}$ and $^{NHOH}L^{-}$, and twisted non-H-bonded phenolate $^{NMe2}L^{-}$ undergo a one-electron oxidation process to their corresponding persistent phenoxyl radical without any significant conformational changes. Yet, large differences ($\Delta E = E_{HB} - E_{NHB}$) in redox potential (0.262 and 0.304 V) are observed between H-bonded (HB) species ($E(^{NHMe}L^{-/\bullet})$ or $E(^{NHOH}L^{-/\bullet})$, respectively) and the non-H-bonded (NHB) one ($E(^{NMe2}L^{-/\bullet})$). These differences correspond to 25.3 and 29.3 kJ mol^{-1} (ca. 6 and 7 kcal mol^{-1}), respectively, and correlate well with the computed differences in the ionisation potentials (IPs) for CH_3CN solutions between H-bonded phenolate ($^{NHMe}L^{-}$ and $^{NHOH}L^{-}$) and non-H-bonded phenolate $^{NMe2}L^{-}$ of 26.0 and 27.0 kJ mol^{-1}, respectively. Because the non-H-bonded $^{NMe2}L^{-}$ and $^{NMe2}L^{\bullet}$ are significantly twisted from planarity, rotational energy in the reduced and oxidised forms (i.e. $\Delta G_{twistred}$ and $\Delta G_{twistox}$, respectively) should be taken into account as well as the H-bonding energies in the reduced and oxidised forms (i.e. ΔG_{HBred} and ΔG_{HBox}, respectively). This leads to the thermochemical cycle depicted in Scheme 3. Because the twist angles of $^{NMe2}L^{-}$ and $^{NMe2}L^{\bullet}$ are sensibly the same, one can crudely assume that $\Delta G_{twistred} = \Delta G_{twistox}$. Then, the difference in ionisation energy ΔE ($E_{HB} - E_{NHB}$), which can be approximate to $E(^{NHR}L^{-/\bullet}) - E(^{NMe2}L^{-/\bullet})$ experimentally determined, is only related to the difference $\Delta\Delta G$ (i.e. $\Delta G_{HBred} - \Delta G_{HBox}$) between the H-bonding strength of the reduced form (ΔG_{HBred}) and that of the oxidised form (ΔG_{HBox}). Most hydrogen bonds are 3–8 kcal mol^{-1}, so the observed difference $\Delta\Delta G$ of about 6–7 kcal mol^{-1} would indicate that the H-bonding interaction in the phenolate form is much stronger that of the corresponding phenoxyl radical form, and thus imply that the H bond in the phenoxyl radical would be relatively weak.

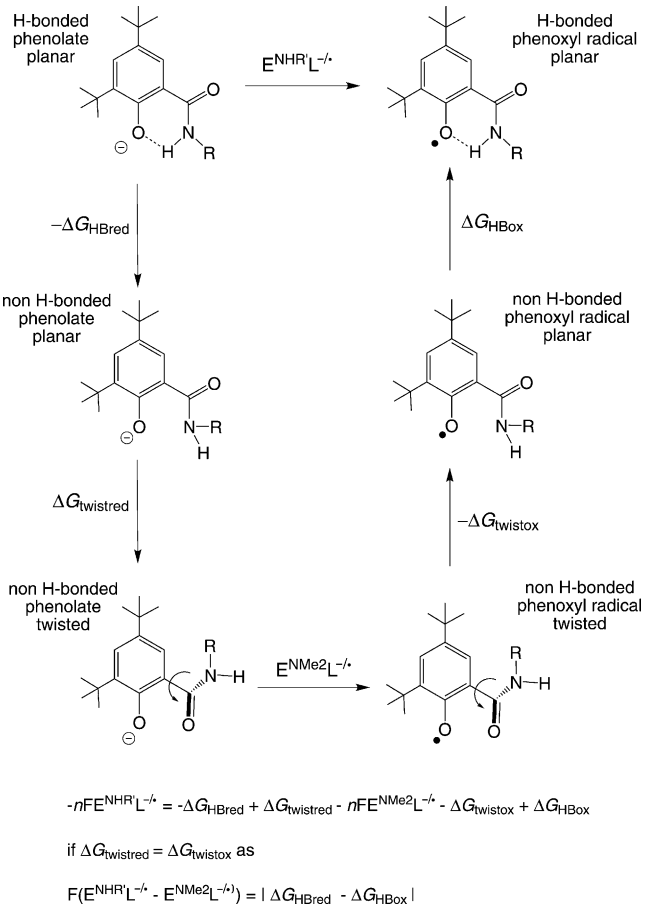

Scheme 3.

The hydrogen-bonding strength is related to the difference in pK_a values between the donor and acceptor; the higher this difference, the weaker the H-bond energy. Upon oxidation from phenolate to the phenoxyl radical, the pK_a decreases from about 10 to about 0, whilst the pK_a of the N–H amide bond is assumed to remain the same (ca. 17). Thus, upon oxidation, the H-bond strength is expected to

decrease significantly, which is consistent with our experimental results.

Biological relevance in enzymatic mechanism: Overall, our findings indicate that there is a large difference in redox potential between H-bonded and non-H-bonded phenolate compounds. This is valuable information in the context of understanding the local environmental factors that modulate the redox potential of the Tyr/Tyr$^{\bullet}$ redox couple in biological systems, and can help to comprehend aspects of enzymatic mechanistic processes. As shown in Scheme 4, we proposed

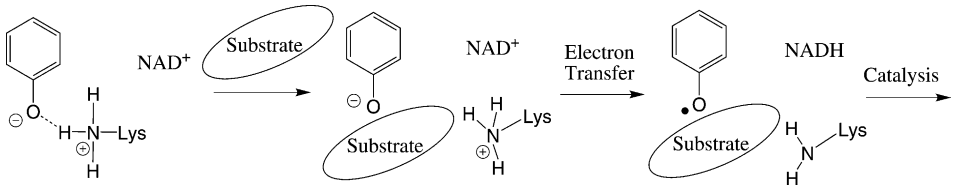

Scheme 4.

a putative mechanism to illustrate this fact. For instance, one could envisage that within an enzyme-active site, the amino acids tyrosine and lysine are located in close proximity. The lysine amine group is more basic than the tyrosine phenol residue, so it is reasonable to propose that the tyrosine is deprotonated (phenolate form) and the lysine is protonated (ammonium form). The two amino acids could establish a H-bonding interaction TyrO$^{-}\cdots$H–NLys of the same type as our model compounds $^{NHMe}L^{-}$ and $^{NHOH}L^{-}$. One could envisage then that conformational changes of the protein under external factors, or more likely substrate binding at the active site, would induce steric constraints and eventually H-bond breaking between the Tyr–Lys conjugate. This in turn would decrease the oxidation potential of the tyrosine, thereby making the oxidation to Tyr$^{\bullet}$ easily achievable through electron transfer to a natural redox cofactor (e.g. FeS clusters, NAD^{+}). Thus, H-bond breaking would trigger the formation of the Tyr$^{\bullet}$, thereby triggering the oxidation catalysis commonly achieved by H atom abstraction from the substrate by the Tyr radical.

Conclusion

We have shown that simple *o*,*p*-*t*Bu-protected salicylamidate compounds can be reversibly oxidised to produce persistent phenoxyl radicals, thus demonstrating that the presence of an amide function at one *ortho* position of the di-*t*Bu-protected phenol ring does not significantly disturb either the stability or the electronic structure of the generated phenoxyl radical, as compared to the 2,4,6-tri-*tert*-butyl phenoxyl radical. The redox potential of these phenolate compounds is strongly influenced by H-bonding. The analyses of the experimental data coupled with theoretical calculations strongly indicate that the effect of the H-bonding on the redox potential is predominantly exerted on the phenolate and not (or only a little) on the phenoxyl radical, in contrast to earlier common belief. As a whole, these compounds constitute valuable chemical models of biological Tyr radicals, and this study also represents a major synthetic development in the chemistry of phenoxyl radicals, as it will enable extensive and versatile synthetic variations or attachments through the amide bond. Further studies towards these goals are in progress in our laboratories.

Experimental Section

General: All syntheses were carried out under an atmosphere of dinitrogen, by using standard Schlenk techniques. All solvents were dried, degassed and distilled prior to use. The reagents *N*-hydroxysuccinimide and dicyclohexylcarbodiimide (Aldrich) were purchased and used without further purification.

C, H and N analyses were carried out by the Microanalytical Service of the Instituto Superior Técnico. Infrared spectra (4000–400 cm^{-1}) were recorded on a BIO-RAD FTS 3000MX instrument in KBr pellets. Frequencies are expressed in cm^{-1}. UV/Vis–NIR spectra (1600–200 nm) were recorded on a Shimadzu UV-3101PC UV/Vis NIR spectrophotometer. ^{1}H, ^{13}C NMR spectra were measured on Bruker 300 and 400 UltraShield spectrometers. ^{1}H and ^{13}C chemical shifts δ are expressed in ppm relative to Si(Me)$_4$. Coupling constants are in Hz; abbreviations: s, singlet; d, doublet; m, complex multiplet.

Electrochemistry: The electrochemical experiments were carried out on an EG&G PAR 273A potentiostat/galvanostat connected to a personal computer through a general-purpose interface bus (GPIB). Cyclic voltammetry studies were undertaken in a two-compartment three-electrode cell, with platinum disk working (d=0.5 mm) and counter electrodes. A Luggin capillary connected to a silver-wire pseudo-reference electrode was used to control the working electrode potential. The solutions were saturated with N_2 by bubbling this gas before each run and were 10^{-3} M in the test compound and 0.2 M in $[NBu_4][BF_4]$ as supporting electrolyte. Controlled potential electrolysis (CPE) was carried out in a two-compartment three-electrode cell with platinum-gauze working and counter electrodes in compartments separated by a glass frit; a Luggin capillary, probing the working electrode, was connected to a silver-wire pseudo-reference electrode. The solutions were saturated with N_2 by bubbling this gas before each run and were 0.2 M in $[NnBu_4][BF_4]$ as supporting electrolyte and approximately 10^{-3} M in the test compound.

Reversibility tests and CPE (in CH_3CN at RT): $[^{NHOH}L][NBu_4]$: $E_{1/2}$ = −0.119 V versus Fc/Fc^{+}, E_p^a = −89 mV, ΔE = 61 mV at 120 mV s^{-1}. ΔE = 58–71 mV (scan rate = 20–900 mV s^{-1}); $i_p^c/i_p^a = 1 \pm 0.1$ at scan rate $\geq$100 mV s^{-1}; at 20, 50 and 80 mV s^{-1}, i_p^c/i_p^a was 1.18, 1.34 and 1.29, respectively; i_p^c (and i_p^a) $\propto$ (scan rate)$^{1/2}$. For Fc/Fc^{+}: ΔE = 60–88 mV (scan rate = 20–900 mV s^{-1}). Thus, the process is considered to be fully reversible. CPE of $[^{NHOH}L][NBu_4]$ performed in acetonitrile at room temperature at 0.360 V versus Ag/AgCl indicated the transfer of 0.97 electrons per molecule. Thus, this is a one-electron oxidation process.

$[^{NMe2}L][NBu_4]$: $E_{1/2}$ = −0.423 V versus Fc/Fc^{+}, E_p^a = −385 mV, ΔE = 77 mV at 120 mV s^{-1}. ΔE = 69–89 mV (scan rate = 20–900 mV s^{-1}); $i_p^c/i_p^a = 1 \pm 0.1$ at scan rate $\geq$100 mV s^{-1}; at 20, 50 and 80 mV s^{-1}, i_p^c/i_p^a was 1.21, 1.21 and 1.33, respectively; i_p^c (and i_p^a) $\propto$ (scan rate)$^{1/2}$. For Fc/Fc^{+}: ΔE = 72–90 mV (scan rate = 20–900 mV s^{-1}). Thus, the process is considered to be fully reversible. CPE of $[^{NMe2}L][NBu_4]$ performed in acetonitrile at room temperature at 0.184 V versus Ag/AgCl indicated the transfer of

0.98 electrons per molecule. Thus, this is a one-electron oxidation process.

[^{NHMe}L][NBu$_4$]: $E_{1/2} = -0.161$ V versus Fc/Fc$^+$, $E_p^a = -129$ mV, $\Delta E =$ 65 mV at 120 mV s^{-1}. $\Delta E = 65$–99 mV (scan rate = 20–900 mV s^{-1}); $i_p^c/i_p^a = 1 \pm 0.1$ at scan rate ≥ 50 mV s^{-1}; at 20, i_p^c/i_p^a was 1.27; i_p^c (and i_p^a) $\propto$ (scan rate)$^{1/2}$. For Fc/Fc$^+$: $\Delta E = 69$–89 mV (scan rate = 20–900 mV s^{-1}). Thus, the process is considered to be fully reversible. CPE of [^{NHMe}L][NBu$_4$] performed in acetonitrile at room temperature at 0.320 V versus Ag/AgCl indicated the transfer of 0.98 electrons per molecule. Thus, this is a one-electron oxidation process.

EPR spectroscopy: EPR spectra were recorded on a Bruker ESP 300E X-band spectrometer equipped with an ER 4111 VT variable-temperature unit; g values were calculated from the formula $\nu = 1.39962\,g\,B'$, in which ν is the frequency measured (GHz) and B' is the corrected value of field (kGauss). The field correction (ΔB) was calculated from the difference between the theoretical and experimental values of field ($B' - B^{exp}$) of our reference compound (i.e. perylene radical in concd. sulfuric acid) with known g value (i.e. 2.002569): $B' = \nu^{exp}/(1.39962\,g)$. [^{NHOH}L]$^\bullet$ (in CH_3CN at 253–270 K): centre field: 3354.3358; modulation frequency: 100 kHz; modulation amplitude: 1.0–0.1 Gpp; receiver gain: 4.48×10^{-4}; conversion time: 40.96 ms; time constant: 81.92 ms; sweep time: 167.77 s. Calculation for 263 K: g values were calculated from the formula $\nu = 1.39962\,g\,B'$, in which ν is the frequency measured (GHz) and B' is the corrected value of field (kGauss). The field correction (ΔB) was calculated from the difference of theoretical and experimental values of field ($B' - B^{exp}$) of our reference compound (i.e. perylene radical in concd. sulfuric acid) with known g value (i.e. 2.002569): $B' = \nu^{exp}/(1.39962\,g)$. Perylene radical in concd. sulfuric acid: $g = 2.002569$; $B^{exp} = 3345.5890$; $\nu^{exp} = 9.409219$ GHz; $B' = 3357.0356$; $\Delta B = 11.4466$. [^{NHOH}L]$^\bullet$: $B^{exp} = 3341.3852$; $\nu^{exp} = 9.405720$ GHz; $B' = 3352.8318$; $g = 2.00433$. [^{NHMe}L]$^\bullet$ (in CH_3CN at 253–270 K): centre field: 3354.6030; modulation frequency: 100 kHz; modulation amplitude: 1.0–0.1 Gpp; receiver gain: 4.48×10^{-4}; conversion time: 40.96 ms; time constant: 81.92 ms; sweep time: 167.77 s. Calculation for 263 K: perylene radical in concd. sulfuric acid: $g = 2.002569$; $B^{exp} = 3347.2468$; $\nu^{exp} = 9.411541$ GHz; $B' = 3357.8641$; $\Delta B = 10.6172$. [^{NHMe}L]$^\bullet$: $B^{exp} = 3343.9866$; $\nu^{exp} = 9.410058$ GHz; $B' = 3354.6038$; $g = 2.00420$. [^{NMe2}L]$^\bullet$ (in CH_3CN at 253–270 K): centre field: 3353.3816; modulation frequency: 100 kHz; modulation amplitude: 1.0–0.1 Gpp; receiver gain: 4.48×10^{-4}; conversion time: 40.96 ms; time constant: 81.92 ms; sweep time: 167.77 s. Calculation for 263 K: perylene radical in concd. sulfuric acid: $g = 2.002569$; $B^{exp} = 3348.1435$; $\nu^{exp} = 9.414326$ GHz; $B' = 3358.8577$; $\Delta B = 10.7142$. [^{NMe2}L]$^\bullet$: $B^{exp} = 3343.2112$; $\nu^{exp} = 9.410179$ GHz; $B' = 3353.9254$; $g = 2.00463$. In all cases the microwave power supplied to the resonator was varied in the range 0.2–2 mW.

DFT calculations: The full geometry optimisation of all structures was carried out at the DFT/Hartree–Fock (HF) hybrid level of theory using Becke's three-parameter hybrid exchange functional in combination with the gradient-corrected correlation functional of Lee, Yang and Parr (B3LYP)[40,41] with the help of the Gaussian 98[42] program package. Restricted approximations for the structures with closed electron shells and unrestricted methods for the structures with open electron shells were employed. No symmetry operations were applied. The standard 6-31+G(d) basis set was used for all atoms. The Hessian matrix was calculated analytically for the optimised structures to prove the location of correct minima (no imaginary frequencies) and to estimate the thermodynamic parameters, the latter being calculated at 25 °C. Several possible conformations were calculated and only the most stable ones are discussed. Total energies corrected for solvent effects (E_s) were estimated at the single-point calculations on the basis of gas-phase geometries using the polarisable continuum model in the CPCM version[43,44] with CH_3CN as solvent. The entropic term in CH_3CN solution (S_s) was calculated according to the procedure described by Wertz[45] and Cooper and Ziegler.[46] Adiabatic ionisation potentials were calculated as the difference of the Gibbs free energies in solution ($G_{s,ox} - G_{s,nox}$) or of the total energies in the gas phase ($E_{g,ox} - E_{g,nox}$), in which the index "nox" corresponds to the non-oxidised species and the index "ox" corresponds to the oxidised species with an unrelaxed geometry.

Crystal structure analysis: Single crystals of ^{NHOH}LH, ^{NMe2}LH, [^{NHOH}L]-[NBu$_4$]·2H$_2$O and [^{NHMe}L][NBu$_4$] were obtained as indicated above. CCDC-782425, 782426, 823791 and 823792 contain the supplementary crystallographic data for this paper. These data can be obtained free of charge from The Cambridge Crystallographic Data Centre via www.ccdc.cam.ac.uk/data_request/cif.

Intensity data were collected at 150 K, by using a Bruker AXS-KAPPA APEX II diffractometer with graphite-monochromated Mo$_{K\alpha}$ ($\lambda = 0.71069$ nm) radiation. Data were collected using omega scans of 0.5° per frame and full spheres of data were obtained. Cell parameters were retrieved by using Bruker SMART software and refined with Bruker SAINT[47] on all the observed reflections. Absorption corrections were applied by using SADABS.[47] Structures were solved by direct methods by using the SHELXS-97 package[48] and refined with SHELXL-97.[49] Calculations were performed with the WinGX System,Version 1.80.03.[50] The NBu$_4^+$ counterion of ^{NHMe}L$^-$ is highly disordered and could not be modelled. PLATON/SQUEEZE[51] was used to correct the data. A potential volume of 2090 Å^3 was found with 587 electrons per unit cell worth of scattering, which fits to the cation. All hydrogen atoms were inserted in calculated positions. Least-squares refinements with anisotropic thermal motion parameters for all the non-hydrogen atoms and isotropic parameters for the remaining atoms were employed.

***N*-3,5-Di-*tert*-butylsalicyloxysuccinimide**: The first step consisted in the elimination of water from commercial 3,5-di-*tert*-butylsalicylic acid monohydrate, by dissolving it in diethyl ether and leaving to dry for 1 day over Na_2SO_4. The solution was then filtered and evaporated to give the dried compound. The latter (10 g, 72.4 mmol) and *N*-hydroxysuccinimide (9.2 g, 79.6 mmol, 1.1 equiv) were dissolved in dioxane (250 mL). The solution was cooled to 0 °C and a solution of dicyclohexylcarbodiimide (16.4 g, 79.6 mmol, 1.1 equiv) in dioxane (200 mL) was added dropwise. The reaction mixture was left stirring at room temperature under an inert atmosphere for 24 h, with formation of a white precipitate (urea derivative). The mixture was filtered using a Buchner funnel and the filtrate was evaporated to dryness to give a white powder in 85% yield. ^{1}H NMR (400 MHz, $CDCl_3$): 10.11 (s, 1H; OH(phenol)), 7.82 (d, $J^4 =$ 2.5 Hz, 1H; ArH), 7.64 (d, $J^4 = 2.5$ Hz, 1H; ArH), 2.92 (s, 4H; -CH_2-CH_2-), 1.41 (s, 9H; *t*Bu), 1.30 ppm (s, 9H; *t*Bu); ^{13}C{^{1}H} NMR (100 MHz, $CDCl_3$): 169.10 (CO), 159.75 (C-, Ar), 141.52 (Ar), 137.82 (Ar), 133.00 (HC(Ar)), 123.40 (HC(Ar)), 107.07 (Ar), 35.23 (C-, *t*Bu), 34.37 (C-, *t*Bu), 31.23 (CH_3, *t*Bu), 29.28 (CH_3, *t*Bu), 25.66 ppm (-CH_2CH_2-).

3,5-Di-*tert*-butyl-2-hydroxy-*N*-(2-hydroxyethyl)benzamide, ^{NHOH}LH: A solution of ethanolamine (0.4 g, 6.7 mmol) in DMF (5 mL) was added to a solution of *N*-3,5-di-*tert*-butylsalicyloxysuccinimide (2.0 g, 5.7 mmol) in DMF (10 mL). Then, triethylamine (6 mL, pre-dried over NaOH) was added to the reaction mixture. After a few minutes a precipitate formed and the reaction mixture was left stirring for 24 h. The mixture was then poured into ice/water 10% HCl (20 mL) and the white precipitate was isolated by filtration through a Buchner funnel, collected and dried under vacuum to give ^{NHOH}LH in 86% yield. ^{1}H NMR (CD_3CN): 13.31 (s, 1H; OH(phenol)), 7.49–7.48 (m, 1H+1H; ArH+NH), 7.41 (d, $J^4 =$ 2.5 Hz, 1H; ArH), 3.86 (broad, 2H; CH_2-OH), 3.46 (q, 2H; CH_2-NHCO), 2.97 (broad, 1H; OH), 1.40 (s, 9H; *t*Bu), 1.31 ppm (s, 9H; *t*Bu); ^{13}C{^{1}H} NMR (100 MHz, $CDCl_3$): 172.01 (CO), 158.67 (C-OH, Ar), 139.90 (C-*t*Bu, Ar), 137.94 (C-*t*Bu, Ar), 128.81 (CH, Ar), 119.69 (CH, Ar), 113.10 (*C*-CO, Ar), 61.86 (CH_2-OH), 42.37 (CH_2-NH), 35.16 (*C*-$(CH_3)_3$), 34.31 (*C*-$(CH_3)_3$), 31.48 (CH_3, *t*Bu), 29.35 ppm (CH_3, *t*Bu); MS (EI (+)): *m*/*z* (%): 294 [*M*+H]$^+$, 316 [*M*+Na]$^+$; IR (KBr pellets): 3486 (N–H), 3313 (PhO–H), 1624 (C=O), 1586, 1554 cm^{-1}; (5 mM sol in CH_3CN): 3411 (N–H), 1634 (C=O) cm^{-1}; elemental analysis calcd (%) for $C_{17}H_{27}NO_3$ (293.19): C 69.59, H 9.28, N 4.77; found: C 69.26, H 8.82, N 4.93.

3,5-Di-*tert*-butyl-2-hydroxy-*N*-dimethylbenzamide, ^{NMe2}LH: A 2.0 M solution in THF of dimethylamine (3.45 mL, 6.9 mmol) diluted with DMF (3 mL) was added to a solution of *N*-3,5-di-*tert*-butylsalicyloxysuccinimide (2.0 g, 5.7 mmol) in DMF (13 mL). Then, triethylamine (3 mL, pre-dried over NaOH) was added to the reaction mixture. After few minutes the mixture became milky and a solid started to form. The suspension was left stirring for 24 h, then poured into ice/water 10% HCl (20 mL) and

the milky final mixture was stirred at 0 °C for 10 min. The white precipitate was removed by filtration through a Buchner funnel, collected and dried under vacuum to give ^{NMe2}LH in 80% yield. ^{1}H NMR (CD_3CN): 10.33 (s, 1H; OH(phenol)), 7.41 (d, J^4 = 2.4 Hz, 1H; ArH), 7.26 (d, J^4 = 2.4 Hz, 1H; ArH), 3.09 (s, 6H; $(CH_3)_2N$), 1.40 (s, 9H; *t*Bu), 1.29 ppm (s, 9H; *t*Bu); ^{13}C{^{1}H} NMR (100 MHz, $CDCl_3$): 173.44 (CO), 159.82 (C-OH, Ar), 139.61 (C-*t*Bu, Ar), 137.52 (C-*t*Bu, Ar), 126.84 (CH, Ar), 123.16 (CH, Ar), 116.42 (*C*-CO, Ar), 36.49 ($(CH_3)_2N$), 35.24 (*C*-$(CH_3)_3$), 34.32 (*C*-$(CH_3)_3$), 31.57 (CH_3, *t*Bu), 29.58 ppm (CH_3, *t*Bu); ^{13}C{^{1}H} NMR (CD_3CN): 173.51 (CO), 156.28 (C-OH, Ar), 140.78 (C-*t*Bu, Ar), 137.74 (C-*t*Bu, Ar), 127.52 (CH, Ar), 124.47 (CH, Ar), 117.84 (*C*-CO, Ar), 38.73 (broad, $(CH_3)_2N$), 35.74 (*C*-$(CH_3)_3$), 34.93 (*C*-$(CH_3)_3$), 31.62 (CH_3, *t*Bu), 29.74 ppm (CH_3, *t*Bu) MS (EI (+)): *m*/*z* (%): 278 [*M*+H]$^+$, 300 [*M*+Na]$^+$; IR (KBr pellets): 3127 (PhO−H), 1612 (C=O), 1586, 1478, 1406 cm^{-1}; (5 mM sol in CH_3CN): 1622 (C=O) cm^{-1}; elemental analysis calcd (%) for $C_{17}H_{27}NO_2$ (277.20): C 73.60, H 9.81, N 5.05; found: C 73.51, H 10.36, N 5.00.

3,5-Di-*tert*-butyl-2-hydroxy-*N*-methylbenzamide, ^{NHMe}LH: A 2.0 M solution in THF of methylamine (4.6 mL, 9.26 mmol) was added to a solution of *N*-3,5-di-*tert*-butylsalicyloxysuccinimide (2.8 g, 8.1 mmol) in DMF (15 mL). Then, triethylamine (8 mL, pre-dried over NaOH) was added to the reaction mixture. After a few minutes the mixture became milky and a solid started to form. The suspension was left stirring for 24 h. After this time the pale yellow mixture was poured into ice/water 10% HCl (30 mL) and the final mixture was stirred at 0 °C for 5 min and filtered through a Buchner funnel. The solid was collected, washed with pentane and dried under vacuum to give ^{NHMe}LH in 82% yield. ^{1}H NMR (CD_3CN): 13.39 (s, 1H; OH(phenol)), 7.47 (d, J^4 = 2.4 Hz, 1H; ArH), 7.37 (m, 1H+1H; ArH+NH), 2.87 (d, J^3 = 4.8 Hz, 3H; H_3C-NH), 1.40 (s, 9H; *t*Bu), 1.30 (s, 9H; *t*Bu); ^{13}C{^{1}H} NMR (100 MHz, $CDCl_3$): 172.01 (CO), 158.71 (C-OH, Ar), 139.93 (C-*t*Bu, Ar), 138.26 (C-*t*Bu, Ar), 128.80 (CH, Ar), 119.15 (CH, Ar), 113.42 (*C*-CO, Ar), 35.32 (*C*-$(CH_3)_3$), 34.41 (*C*-$(CH_3)_3$), 31.62 (CH_3, *t*Bu), 29.50 (CH_3, *t*Bu), 26.65 ppm (H_3C-N); ^{13}C{^{1}H} NMR (CD_3CN): 172.70 (CO), 159.40 (C-OH, Ar), 140.89 (C-*t*Bu, Ar), 138.11 (C-*t*Bu, Ar), 129.24 (CH, Ar), 121.40 (CH, Ar), 114.34 (*C*-CO, Ar), 35.71 (*C*-$(CH_3)_3$), 35.04 (*C*-$(CH_3)_3$), 31.67 (CH_3, *t*Bu), 29.61 (CH_3, *t*Bu) 26.32 ppm (H_3C-N); MS (EI (+)): *m*/*z* (%): 264 [*M*+H]$^+$, 286 [*M*+Na]$^+$; IR (KBr pellets): 3419 (N−H), 3328 (PhO−H), 1620 (C=O), 1582, 1544 cm^{-1}; (5 mM sol in CH_3CN): 3413 (N−H), 1639 (C=O) cm^{-1}; elemental analysis calcd (%) for $C_{16}H_{25}NO_2$ (263.18): C 72.96, H 9.57, N 5.32; found: C 72.89, H 10.09, N 5.29.

2,4-Di-*tert*-butyl-6-(2-hydroxyethylcarbamoyl)phenolate tetrabutylammonium salt, [^{NHOH}L][NBu_4]: A 1.0 M solution in methanol of tetrabutylammonium hydroxide (5.1 mL, 5.1 mmol) was added to a solution of 3,5-di-*tert*-butyl-2-hydroxy-*N*-(2-hydroxyethyl)benzamide (1.5 g, 5.1 mmol) in dry methanol (10 mL). The transparent solution was stirred under N_2 atmosphere for 5 h. Then the solvent was removed under vacuum leaving a white power that was crystallised from CH_2Cl_2/Et_2O to give the corresponding salt [^{NHOH}L][NBu_4] in 72% yield. ^{1}H/^{15}N-HSQC (CD_3CN) and ^{1}H NMR (CD_3CN): 13.90 (br, 1H; NH), 7.63 (br, 1H; ArH), 7.13 (br, 1H; ArH), 5.65 (br, 1H; OH), 3.58 (m, 2H; CH_2-OH), 3.42 (m, 2H; CH_2-NHCO), 3.10–3.04 (m, 8H; -CH_2-N, [NBu_4]), 1.65–1.54 (m, 8H; -CH_2-, [NBu_4]), 1.39–1.30 (m, 9H+8H; *t*Bu+[NBu_4]), 1.25 (s, 9H; *t*Bu), 0.99–0.93 ppm (m, 12H; CH_3-, [NBu_4]); ^{13}C{^{1}H} NMR (100 MHz, $CDCl_3$): 172.18 (CO), 157.77 (*C*-O$^-$, Ar), 137.72 (C-*t*Bu, Ar), 136.10 (C-*t*Bu, Ar), 127.42 (HC(Ar)), 122.19 (HC(Ar)), 114.75 (*C*-CO, Ar), 61.76 (CH_2-OH), 58.53 (-CH_2-N, [NBu_4]), 42.77 (CH_2-NH), 35.03 (C-, *t*Bu), 34.12 (C-, *t*Bu), 31.64 (CH_3, *t*Bu), 29.54 (CH_3, *t*Bu), 23.80 (-CH_2-, [NBu_4]), 19.54 (-CH_2-, [NBu_4]), 13.53 ppm (-CH_3, [NBu_4]); MS (EI (−)): *m*/*z* (%): 292 [^{NHOH}L]$^-$; MS (EI (+)): *m*/*z* (%): 242 [NBu_4]$^+$; IR (KBr pellets): 3400 (CH_2O−H), 3114 (N−H), 1617 (C=O), 1584 cm^{-1}; (5 mM sol in CH_3CN): 3005 (N−H), 2966, 1624 (C=O), 1572 cm^{-1}; elemental analysis calcd (%) for $C_{33}H_{62}N_2O_3$ (534.47): C 74.11, H 11.68, N 5.24; found: C 74.10, H 12.48, N 5.33. X-ray-quality single crystals were grown by slow diffusion of dry diethyl ether in a concentrated solution of the title compound in dichloromethane, under a dinitrogen atmosphere.

2,4-Di-*tert*-butyl-6-(2-dimethylcarbamoyl)phenolate tetrabutylammonium salt, [^{NMe2}L][NBu_4]: A 1.0 M solution in methanol of tetrabutylammonium hydroxide (7.2 mL, 7.2 mmol) was added to a solution of 3,5-di-*tert*-butyl-2-hydroxy-*N*-dimethylbenzamide (2 g, 7.2 mmol) in dry methanol (10 mL). The colourless solution turned pale yellow and was stirred under N_2 atmosphere for 5 h. Then the solvent was removed under vacuum leaving a yellow oil. This crude oil was suspended in Et_2O, the mixture was stirred for 2 h and the solvent was gently decanted off. The residue was dried under vacuum to leave the corresponding salt [^{NMe2}L]-[NBu_4] in 89% yield. ^{1}H NMR (400 MHz, CD_3CN): 7.69 (br, 1H; ArH), 7.23 (br, 1H; ArH), 3.11–3.05 (m, 8H; -CH_2-N, [NBu_4]), 2.98 (s, 6H,; $(CH_3)_2$-N), 1.64–1.53 (m, 8H; -CH_2-, [NBu_4]), 1.39–1.29 (m, 9H+8H; *t*Bu+[NBu_4]), 1.24 (s, 9H; *t*Bu), 1.00–0.94 ppm (m, 12H; CH_3-, [NBu_4]); ^{13}C{^{1}H} NMR (100 MHz, $CDCl_3$: 173.10 (CO), 159.01 (C-O$^-$, Ar), 138.26 (C-*t*Bu, Ar), 136.76 (C-*t*Bu, Ar), 126.11 (CH, Ar), 124.39 (CH, Ar), 117.24 (*C*-CO, Ar), 59.12 (-CH_2-N, [NBu_4]), 36.21 ($(CH_3)_2N$), 35.87 (*C*-$(CH_3)_3$), 34.98 (*C*-$(CH_3)_3$), 31.23 (CH_3, *t*Bu), 29.65 (CH_3, *t*Bu), 23.71 (-CH_2-, [NBu_4]), 19.64 (-CH_2-, [NBu_4]), 13.48 ppm (-CH_3, [NBu_4]); MS (EI (−)): *m*/*z* (%): 262 [^{NMe2}L]$^-$; MS (EI (+)): *m*/*z* (%): 242 [NBu_4]$^+$; IR (nujol): 1638 (C=O) cm^{-1}; (5 mM sol in CH_3CN): 1633 (C=O) cm^{-1}; elemental analysis calcd (%) for $C_{33}H_{62}N_2O_2$ (518.47): C 76.40, H 12.04, N 5.40; found.: C 76.75, H 12.32, N 5.21.

2,4-Di-*tert*-butyl-6-(2-methylcarbamoyl)phenolate tetrabutylammonium salt, [^{NHMe}L][NBu_4]: A 1.0 M solution in methanol of tetrabutylammonium hydroxide (3.8 mL, 3.8 mmol) was added to a solution of 3,5-di-*tert*-butyl-2-hydroxy-*N*-methylbenzamide (1 g, 3.8 mmol) in dry methanol (5 mL). The colourless solution turned pale yellow and was stirred under N_2 atmosphere for 5 h. Then the solvent was removed under vacuum leaving a yellow oil. This crude oil was suspended in Et_2O, the mixture was stirred for 2 h and the solvent was gently decanted off. The sticky off-white solid was dried under vacuum to leave the corresponding salt [^{NHMe}L][NBu_4] in quantitative yield. ^{1}H NMR (400 MHz, CD_3CN): 13.20 (br, 1H; NH), 7.63–7.08 (br, 2H; ArH), 3.08–3.04 (m, 8H; -CH_2-N, [NBu_4]), 2.80 (s, 3H; CH_3-NH), 1.61–1.54 (m, 8H; -CH_2-, [NBu_4]), 1.38–1.29 (m, 9H+8H; *t*Bu+[NBu_4]), 1.23 (s, 9H; *t*Bu), 0.97 ppm (t, J^3 = 7.0 Hz, 12H; CH_3-, [NBu_4]); ^{13}C{^{1}H}-NMR (100 MHz, CD_3CN): 172.34 (CO), n.d. (*C*-O$^-$, Ar), 139.52 (C-*t*Bu, Ar), 128.43 (C-*t*Bu, Ar), 125.86 (HC(Ar)), 124.04 (HC(Ar)), 59.19 (-CH_2-N, [NBu_4]), 35.85 (C-, *t*Bu), 34.23 (C-, *t*Bu), 32.32 (CH_3, *t*Bu), 29.93 (CH_3, *t*Bu), 25.32 (CH_3-NH), 24.23 (-CH_2-, [NBu_4]), 20.24 (-CH_2-, [NBu_4]), 13.74 ppm (-CH_3, [NBu_4]); MS (EI (−)): *m*/*z* (%): 262 [^{NHMe}L]$^-$; MS (EI (+)): *m*/*z* (%): 242 [NBu_4]$^+$; IR (KBr pellets): 3274 (N−H), 1623 (C=O), 1584 cm^{-1}; (5 mM sol in CH_3CN): 3009 (N−H), 1626 (C=O) cm^{-1}; elemental analysis calcd (%) for $C_{32}H_{60}N_2O_2$ (504.47): C 76.13, H 11.97, N 5.55; found: C 75.63, H 10.20, N 5.90. X-ray-quality single crystals were grown by slow diffusion of dry diethyl ether in a concentrated solution of the title compound in dichloromethane, under a dinitrogen atmosphere.

Acknowledgements

This work was partially supported by the Foundation for Science and Technology (FCT) for the grants SFRH/BD/23187/2005 and SFRH/BPD/70953/2010 (R.W.). Dr. J. P. Telo and Dr. M. C. Oliviera are also acknowledged for assistance with EPR and MS measurements.

[1] J. Stubbe, W. A. van der Donk, *Chem. Rev.* **1998**, *98*, 705.
[2] K. E. Silva, T. E. Elgren, L. Que, M. T. Stankovich, *Biochemistry* **1995**, *34*, 14093.
[3] I. Vass, S. Styring, *Biochemistry* **1991**, *30*, 830.
[4] T. Maki, Y. Araki, Y. Ishida, O. Onomura, Y. Matsumura, *J. Am. Chem. Soc.* **2001**, *123*, 3371.
[5] I. J. Rhile, J. M. Mayer, *J. Am. Chem. Soc.* **2004**, *126*, 12718.
[6] F. Thomas, O. Jarjayes, M. Jamet, S. Hamman, E. Saint-Aman, C. Duboc, J. L. Pierre, *Angew. Chem.* **2004**, *116*, 604; *Angew. Chem. Int. Ed.* **2004**, *43*, 594.

[7] L. Benisvy, R. Bittl, E. Bothe, C. D. Garner, J. McMaster, S. Ross, C. Teutloff, F. Neese, *Angew. Chem.* **2005**, *117*, 5448; *Angew. Chem. Int. Ed.* **2005**, *44*, 5314.
[8] I. J. Rhile, J. M. Mayer, *Angew. Chem.* **2005**, *117*, 1624; *Angew. Chem. Int. Ed.* **2005**, *44*, 1598.
[9] L. Benisvy, E. Bill, A. J. Blake, D. Collison, E. S. Davies, C. D. Garner, G. McArdle, E. J. L. McInnes, J. McMaster, S. H. K. Ross, C. Wilson, *Dalton Trans.* **2006**, 258.
[10] C. Costentin, M. Robert, J. M. Saveant, *J. Am. Chem. Soc.* **2006**, *128*, 4552.
[11] I. J. Rhile, T. F. Markle, H. Nagao, A. G. DiPasquale, O. P. Lam, M. A. Lockwood, K. Rotter, J. M. Mayer, *J. Am. Chem. Soc.* **2006**, *128*, 6075.
[12] L. Benisvy, D. Hammond, D. J. Parker, E. S. Davies, C. D. Garner, J. McMaster, C. Wilson, F. Neese, E. Bothe, R. Bittl, C. Teutloff, *J. Inorg. Biochem.* **2007**, *101*, 1859.
[13] T. F. Markle, J. M. Mayer, *Angew. Chem.* **2008**, *120*, 750; *Angew. Chem. Int. Ed.* **2008**, *47*, 738.
[14] T. F. Markle, I. J. Rhile, A. G. DiPasquale, J. M. Mayer, *Proc. Natl. Acad. Sci. USA* **2008**, *105*, 8185.
[15] J. J. Warren, T. A. Tronic, J. M. Mayer, *Chem. Rev.* **2010**, *110*, 6961.
[16] C. A. Jiménez, J. B. Belmar, *Tetrahedron* **2005**, *61*, 3933.
[17] D. Kanamori, T. A. Okamura, H. Yamamoto, N. Ueyama, *Angew. Chem.* **2005**, *117*, 991; *Angew. Chem. Int. Ed.* **2005**, *44*, 969.
[18] D. Kanamori, A. Furukawa, T. Okamura, H. Yamamoto, N. Ueyama, *Org. Biomol. Chem.* **2005**, *3*, 1453.
[19] One should note that, whilst crystals of $[^{NHOH}L][NBu_4]\cdot 2H_2O$ contain water molecules, which establish an H-bonding network (see Figure SI2, Supporting Information), the bulk organic salt does not contain water, as evidenced by the NMR, IR and micronalysis characterisations. In $[^{OHNH}L][NBu_4]\cdot 2H_2O$, quasi-planar dimers are formed through mutual intermolecular H-bonding interaction between the alcohol pendant arm O(3)–H(3) of one molecule and phenolate–O(1) from another molecule. The latter dimers $[^{NHOH}L]_2$ are connected through H-bonding with tetramer water clusters (Figure SI2a), thereby giving rise to a hydrophilic H-bonding chain sandwiched by a hydrocarbon shell generated by the *tert*-butyl groups. The arrangement of cations and anions in these organic salts is different (Figure SI2b). In $[^{NHOH}L][NBu_4]\cdot 2H_2O$ the hydrophobic NBu_4 cations are sandwiched between hydrophilic chains generated from the ^{NHOH}L anions and the water molecules (Figure SI2b). The ^{NHOH}L anions in $[^{NHOH}L][NBu_4]$ can be envisaged as trapped in nutshells of hydrophobic NBu_4 cations (Figure SI3).
[20] G. A. Jeffrey, *An Introduction to Hydrogen Bonding*, Oxford University Press, Oxford, **1997**.
[21] D. Kanamori, T. Okamura, H. Yamamoto, S. Shimizu, Y. Tsujimoto, N. Ueyama, *Bull. Chem. Soc. Jap.* **2004**, *77*, 2057.
[22] a) L. Benisvy, I. Mutikainen, M. Quesada, U. Turpeinen, P. Gamez, J. Reedijk, *Chem. Commun.* **2006**, 3723; b) L. Benisvy, P. Gamez, W. T. Fu, H. Kooijman, A. L. Spek, A. Meijerink, J. Reedijk, *Dalton Trans.* **2008**, 3147.
[23] C. Xie, P. M. Lahti, C. George, *Org. Lett.* **2000**, *2*, 3417.
[24] M. A. Hossain, F. Thomas, S. Hamman, E. Saint-Aman, D. Boturyn, P. Dumy, *J. Pept. Sci.* **2006**, *12*, 612.
[25] F. G. Bordwell, J. P. Cheng, *J. Am. Chem. Soc.* **1991**, *113*, 1736.
[26] M. Lucarini, V. Mugnaini, G. F. Pedulli, *J. Am. Chem. Soc.* **2003**, *125*, 8318.
[27] P. J. O'Malley, *J. Am. Chem. Soc.* **1998**, *120*, 11732.
[28] M. Engström, F. Himo, A. Graslund, B. Minaev, O. Vahtras, H. Agren, *J. Phys. Chem. A* **2000**, *104*, 5149.
[29] M. Kaupp, T. Gress, R. Reviakine, O. L. Malkina, V. G. Malkin, *J. Phys. Chem. B* **2003**, *107*, 331.
[30] J. R. Asher, N. L. Doltsinis, M. Kaupp, *J. Am. Chem. Soc.* **2004**, *126*, 9854.
[31] S. Un, M. Atta, M. Fontecave, A. W. Rutherford, *J. Am. Chem. Soc.* **1995**, *117*, 10713.
[32] P. Faller, C. Goussias, A. W. Rutherford, S. Un, *Proc. Natl. Acad. Sci. USA* **2003**, *100*, 8732.
[33] F. Lachaud, A. Quaranta, Y. Pellegrin, P. Dorlet, M.-F. Charlot, S. Un, W. Leibl, A. Aukauloo, *Angew. Chem.* **2005**, *117*, 1560; *Angew. Chem. Int. Ed.* **2005**, *44*, 1536.
[34] A. L. Maniero, V. Chis, A. Zoleo, M. Brustolon, A. Mezzetti, *J. Phys. Chem. B* **2008**, *112*, 3812.
[35] a) P. J. van Dam, J. P. Willems, P. P. Schmidt, S. Potsch, A. L. Barra, W. R. Hagen, B. M. Hoffman, K. K. Andersson, A. Graslund, *J. Am. Chem. Soc.* **1998**, *120*, 5080; b) I. Garcia-Bosch, A. Company, C. W. Cady, S. Styring, W. R. Browne, X. Ribas, M. Costas, *Angew. Chem.* **2011**, *123*, 5766–5771; *Angew. Chem. Int. Ed.* **2011**, *50*, 5648–5653.
[36] P. Dorlet, A. W. Rutherford, S. Un, *Biochemistry* **2000**, *39*, 7826.
[37] P. Allard, A. L. Barra, K. K. Andersson, P. P. Schmidt, M. Atta, A. Graslund, *J. Am. Chem. Soc.* **1996**, *118*, 895.
[38] E. R. Altwicker, *Chem. Rev.* **1967**, *67*, 475.
[39] E. Land, G. Porter, E. Strachan, *Trans. Faraday Soc.* **1961**, *57*, 1885.
[40] A. D. Becke, *J. Chem. Phys.* **1993**, *98*, 5648.
[41] C. Lee, W. Yang, R. G. Parr, *Phys. Rev. B* **1988**, *37*, 785.
[42] Gaussian 98 (Revision A.9), M. J. Frisch, G. W. Trucks, H. B. Schlegel, G. E. Scuseria, M. A. Robb, J. R. Cheeseman, V. G. Zakrzewski, J. A. Montgomery, Jr., R. E. Stratmann, J. C. Burant, S. Dapprich, J. M. Millam, A. D. Daniels, K. N. Kudin, M. C. Strain, O. Farkas, J. Tomasi, V. Barone, M. Cossi, R. Cammi, B. Mennucci, C. Pomelli, C. Adamo, S. Clifford, J. Ochterski, G. A. Petersson, P. Y. Ayala, Q. Cui, K. Morokuma, D. K. Malick, A. D. Rabuck, K. Raghavachari, J. B. Foresman, J. Cioslowski, J. V. Ortiz, B. B. Stefanov, G. Liu, A. Liashenko, P. Piskorz, I. Komaromi, R. Gomperts, R. L. Martin, D. J. Fox, T. Keith, M. A. Al-Laham, C. Y. Peng, A. Nanayakkara, C. Gonzalez, M. Challacombe, P. M. W. Gill, B. G. Johnson, W. Chen, M. W. Wong, J. L. Andres, M. Head-Gordon, E. S. Replogle, J. A. Pople, Gaussian, Inc., Pittsburgh, PA, **1998**.
[43] J. Tomasi, M. Persico, *Chem. Rev.* **1994**, *94*, 2027.
[44] V. Barone, M. Cossi, *J. Phys. Chem. A* **1998**, *102*, 1995.
[45] D. H. Wertz, *J. Am. Chem. Soc.* **1980**, *102*, 5316.
[46] J. Cooper, T. Ziegler, *Inorg. Chem.* **2002**, *41*, 6614.
[47] Bruker, APEX2 & SAINT, Madison, Wisconsin, **2004**.
[48] G. M. Sheldrick, *Acta Crystallogr. Sect. A* **1990**, *46*, 467.
[49] G. M. Sheldrick, *Acta Crystallogr. Sec. A* **2008**, *64*, 112.
[50] L. J. Farrugia, *J. Appl. Crystallogr.* **1999**, *32*, 837.
[51] A. L. Spek, *Acta Crystallogr. Sect. C* **1990**, *46*, C34.

Received: May 16, 2011
Published online: September 5, 2011

